Ordered sigma-type phase in the Ising model of Fe-Cr stainless steel

G. J. Ackland*
School of Physics, CSEC and SUPA, The University of Edinburgh, Mayfield Road, Edinburgh EH9 3JZ, United Kingdom
(Received 25 August 2008; revised manuscript received 9 February 2009; published 27 March 2009)

A lattice-based Ising model is presented which describes precipitation of an ordered phase at high temperature. It is based around the Ising model of mixed ferromagnetism (FM) and antiferromagnetism (AFM), which gives a qualitative description of the FeCr phase diagram. In addition to spin and species, a third index labels the precipitate phase and serves to produce its additional entropy. Thus the FM-AFM Ising model is adapted to produce precipitation of a sigma-type phase at high temperature, as observed in FeCr, in a form suitable for kinetic Monte Carlo simulations. In addition, the anomalous asymmetry observed in the miscibility gap of materials such as FeCr is also described, as is the finite low-temperature solubility and the onset of the stainless property for high-Cr content steel.

DOI: 10.1103/PhysRevB.79.094202 PACS number(s): 64.70.kd, 61.72.Qq, 64.60.−i

I. INTRODUCTION

The appearance of a disordered phase at high temperature is commonplace in intermetallic alloys. However in some systems, such as FeCr, one ordered phase exists at low temperatures and another at high temperatures (440 °C), with disorder ultimately occurring at even higher temperature. This gives a complicated phase diagram: published experimental phase diagrams show at least seven distinct phase or phase-coexistence regions, with some works having as many as 11 distinct regions.[1–3] In this paper we show that such a complex phase diagram can be reproduced by an Ising-type model with just three labels associated with each lattice site.

The Ising model is the simplest model for a phase transformation taking place on a lattice. In its classic form, it describes the transition from ordered to disordered phases. The original motivation was the energetics of magnetism, but the Ising Hamiltonian can also be motivated by many natural phenomena involving short-range interactions between two-state sites. Here, an Ising-type model is used to represent spin (up or down), species (Fe or Cr), and local environment (bcc-like or sigma-like).

FeCr exhibits spinodal decomposition and a miscibility gap[1–4] with a high-T ordered complex structure, the sigma phase, but no known ground-state intermetallic compounds. Curiously, the heat of solution of dilute Cr in Fe is negative,[5–9] so the miscibility gap is skewed to allow high-Cr concentration in the Fe-rich phase and a finite solubility at zero temperature. This is accompanied by pronounced short-ranged order in the solid solution phase.[3,10] This is impossible to describe with pair-potential or embedded-atom-type models[11] and does not appear to be associated with vibrational entropy.[12] Previous works have attempted explanations at various levels of theory, from first-principles, spin-dependent, density-functional theory (DFT) to concentration-dependent interatomic potentials and two-band second-moment tight-binding models.[6–8,13–20] Determining full phase diagrams from such models is computationally expensive and can reveal surprising instabilities.[21,22] Conventional Monte Carlo simulation with density dependent potentials now reproduces the $\alpha-\alpha'$ separation.[23,24]

It is now established that the interplay between Fe-Fe ferromagnetic (FM) and Fe-Cr/Cr-Cr antiferromagnetic (AFM) interactions is key to determining the phase diagram. This focus on the spin-dependent interactions sets the system apart from those where the first departure from a pairwise model is to consider concentration dependence[25] or cluster expansions.[26]

The FM-AFM Ising model is the simplest model which gives this anomalous skewed solubility: this is due to frustration of Cr spins, which cannot be antiparallel both with the Fe matrix and among themselves.[27] The solubility limit of Cr at $T=0$ K is determined by the range of the interaction between two single Cr impurities. According to electronic structure calculations, this interaction extends at similar order of magnitude to fifth-neighbor interactions,[7,28,29] i.e., shells at $(\frac{1}{2},\frac{1}{2},\frac{1}{2})$, (100), (110), $(\frac{3}{2},\frac{1}{2},\frac{1}{2})$, and (111) with 8, 6, 12, 24, and 8 atoms, respectively: a total of 58. This is consistent with a proposed cubic ordered $Fe_{15}Cr$ compound,[8] but this does not appear to be a true ground state.[7,30] Here it is shown that more quantitative agreement between the FM/AFM model and the FeCr phase diagram can be obtained by increasing the range of the interactions to fifth neighbors.

Ferritic stainless steels have good corrosion resistance, high-temperature behavior, and irradiation damage resistance and so are a potential first wall material in nuclear reactors.[31–33] This has sparked an enormous effort in multiscale modeling, linking various methodologies applicable at different lengths and time scales. Within this scheme, atomistic models of structural evolution over time scales of years can only be obtained using kinetic Monte Carlo[34,35] (KMC), which can be applied only to a lattice-based model. Many of the important processes in radiation damage on long time scales involve interstitial defects and incoherent precipitates, and it is therefore essential to generate new lattice-based models which can represent off-lattice features in the KMC framework.

The sigma phase is an approximately 50-50 phase[36] in the case of FeCr alloys. It exists only at high temperatures[37,38] implying that it has higher entropy than the bcc-based phase-separated mixture. Since the sigma phase is paramagnetic[39] (PM), spin is likely to be responsible for the excess entropy, although electronic and vibrational degrees of freedom may also play a role. Short-ranged weak paramagnetic interactions[39] give a Curie temperature around 40 K, rising

somewhat in nanocrystals[40,41] and therefore presumably in microprecipitates. The sigma phase is also found in FeV, and off-stoichiometry in OsW, MoRu, RuW, and MoOs. Although site ordered at low temperatures,[42] the sigma phase has some site disorder at higher temperatures; low antisite defect energy also manifests itself as a range of alloy composition.

The purpose of the present work is twofold, first to determine the minimal mathematical picture that will give a system with anomalous solubility, short-ranged order, and high-temperature ordered phase and to do so in a form suitable for time-efficient computation (i.e., lattice KMC). Second, to relate this to the correct physics (magnetism, species ordering, and the different electronic environment associated with bcc and sigma). Using a lattice model means that the coordination of the high-temperature phase will not correspond to sigma FeCr, but implicit differences in bonding can be described alongside explicit treatment of paramagnetism.

The main result presented here will be to show that a small extension to the AFM/FM Ising model can incorporate a high-temperature ordered PM phase. Everything remains on a bcc lattice, which means that precipitation is directly applicable in KMC calculations once the migration rates are known. Although this work primarily presents a Monte Carlo procedure for high-temperature ordering, for definitiveness, we will describe the model that simulates the thermodynamics of Fe-Cr alloys.

II. ANOMALOUS SOLUBILITY

First we consider the FM-AFM phase diagram without sigma and establish the correct solubility limit for Fe-Cr alloys. The energy of an atom i in the FM/AFM Hamiltonian[27] can be written as

$$H_i^0(N) = \sum_{j=1}^{N} H_{ij}^0, \tag{1}$$

where H_{ij}^0 depends on the species of atoms i and j,

$$H_{ij}^0 = A_N \sigma_i \sigma_j, \quad S_i + S_j = 2 \quad (\mathrm{CrCr}),$$

$$H_{ij}^0 = \sigma_i \sigma_j, \quad S_i + S_j = 0 \quad (\mathrm{CrFe}),$$

$$H_{ij}^0 = -\sigma_i \sigma_j, \quad S_i + S_j = -2 \quad (\mathrm{FeFe}),$$

where S_i label the species ($S_{\mathrm{Cr}}=1$, $S_{\mathrm{Fe}}=-1$), $\sigma_i = \pm 1$ labels the spins, and N is the number of interacting neighbors. The parameter A_N can be adjusted to give a reasonable ratio between Curie and Néel temperatures in iron and chromium, respectively. The overall energy scale is then set by the CrFe and FeFe interactions, which are set to 1.

Finite temperature equilibrium is found by using a Monte Carlo procedure with the Metropolis algorithm, typically over 54 000 sites, with larger systems used close to the phase boundary. For canonical simulations the trial Monte Carlo switch of a randomly chosen site uses Glauber dynamics for the spins and Kawasaki dynamics for the species,

$$\sigma_i \rightarrow -\sigma_i,$$

$$S_i \rightarrow S_j, \quad S_j \rightarrow S_i. \tag{2}$$

Trial moves are accepted with the usual Metropolis probability $\max[\exp(-\Delta E/T), 1]$, which defines the reduced units for the temperature. The process is repeated until equilibrium is found, the temperature is then incremented, and the simulation continues through the phase transition.

The solubility limit of the Cr in Fe at $T=0$ K is determined by the range of the interaction. Including second neighbors ($N=14$ in bcc) gives a DO_3 Fe_3Cr compound without any frustration-inducing Cr-Cr interactions.[27] Consequently the solubility limit at 0 K is 25%, and there is continuous solid solubility between bcc Fe and DO_3/Fe_3Cr. For all concentrations between 0% and 25% there are degenerate ground states for any arrangements where no pairs of Cr atoms are first or second neighbors. This solubility limit is well above the 6% implied by *ab initio* work.

First-principles calculations[6–8] show that the Cr-Cr interaction range extends at least to fifth neighbors.[43] Applying this in Eq. (1) (i.e., $N=58$) gives a 0 K solubility limit of 6.25%, at which concentration there are numerous structures without Cr-Cr distances within the fifth-neighbor separation. This again leads to degenerate periodic and nonperiodic ground states.

With $N=58$ there is significant AFM frustration in pure Cr, and the $T=0$ ground state is a $q=(200)$ spin wave [as can be seen at higher temperature in Fig. 3(a)] which has energy $-10A_{58}$ compared with the FM Fe energy of -58. To maintain a reasonable ratio of Néel to Curie temperature, we choose the largest integer which gives a cohesive energy for Cr smaller than for Fe, $A_{58}=5$, noting that in the real system this energy difference arises from the exchange interaction strength rather than the spin itself. The phase diagram of this fifth-neighbor model has been calculated and gives a good description of the FeCr system aside from the missing sigma phase (Fig. 1).

It is worth noting that if *ab initio* data are used to build a phase diagram using a nonpairwise model in the cluster-variation method, it is essential to incorporate long-ranged clusters.[26] The Ising model is, essentially, a cluster model incorporating only pairwise clusters, and thus one conclusion of this work is that associating energy with larger clusters is not necessary to reproduce the phase diagram, but long-range interactions are. This may be a useful heuristic for producing interatomic potentials for the FeCr system.

III. SURFACE SEGREGATION

Next, we examine the stainless-steel effect. It is well established that chromium confers corrosion resistance in steel when present at above 15%. This is due to surface segregation and subsequent oxide formation. Surprisingly, recent DFT calculations[45–49] showed that Cr segregation to the surface of pure iron was not favorable either entropically[45,46] or energetically,[47,48] except in simulations with small cells.[48,49]

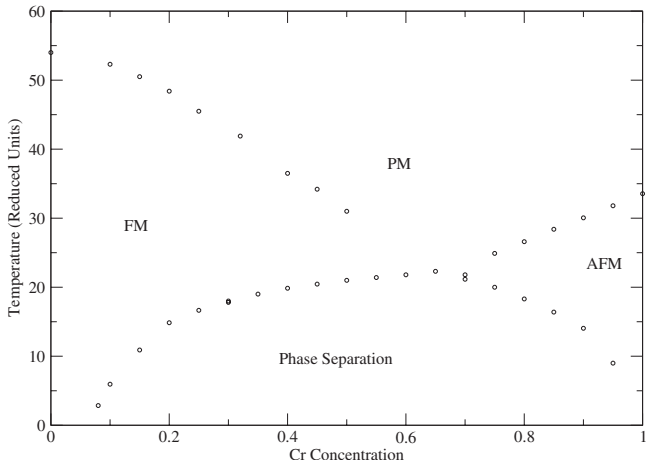

FIG. 1. Phase diagram for fifth-neighbor FM/AFM Ising model on a bcc lattice [Eq. (1), $A_N=5$]. Points are peaks in variance of the energy as a function of temperature (in dimensionless units) and calculated from 40 000 updates on each of 54 000 sites. The skew in the miscibility gap implies solubility of Cr in Fe of 6.25% at $T=0$.

No consideration of surface physics or oxidization is included in the model, thus the results in this section are deduced entirely from the bulk phases and are free of any empirical fitting: we can expect only a qualitative picture. In particular, chemical potentials and onsite terms in the Hamiltonian may be crucial. The chemical potential depends on the external environment; so to avoid ambiguity here we work in the canonical ensemble, so that the composition is fixed and any surface segregation is at the expense of depletion elsewhere.

Figure 2 shows calculations with Eq. (1) of the segregation profile of Cr near the (001) surface for various temperatures and concentrations. Comparison with the phase diagram shows that Cr segregation occurs only for conditions in

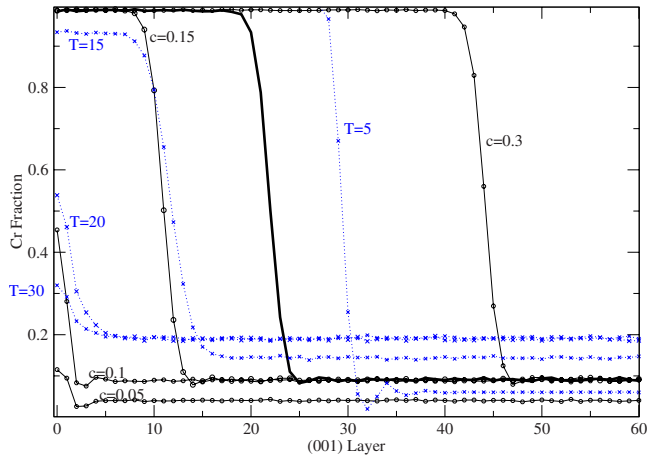

FIG. 2. (Color online) Fraction of Cr atoms against depth using Eq. (1) ($N=58$, $A_{58}=5$). Each simulation used comprised a $20\times20\times100$ supercell oriented on (001). The thick line has reference composition, $C=0.2(Fe_{80}Cr_{20})T=10$. Dotted blue lines/crosses correspond to different temperatures $C=0.2$; solid black lines/circles correspond to different compositions $T=10$.

the phase-separation region: Cr precipitates preferentially at the surface. Thus Cr does not surface segregate in pure iron; the bulk must already be saturated solid solution. This illuminates results from previous *ab initio* calculations: with a single Cr atom, small cells[48] have higher effective Cr concentration than those with larger cells: finite cell size determines which region of the phase diagram the system lies in.

For all temperatures and bulk concentrations a small increase in Cr concentration at the topmost layer can be observed. This is a finite-size effect: isolated surface Cr atoms will have fewer unfavorable Cr neighbors than bulk Cr atoms simply because they have fewer neighbors in total. However this region of enhanced Cr cannot spread into the bulk (the surface effect is lost) or increase to 100% coverage (extra Cr neighbors are unfavored). Experiment suggests that the Cr-enhanced region is a few nanometers thick,[50] and this geometric effect cannot produce more than a monolayer of Cr enhancement.

Once the concentration reaches the phase boundary, precipitation begins in the bulk material. In the surface case, the precipitate nucleates preferentially at the surface: in our calculations we see only a small number of precipitates, usually only those at the surface. Although the model does not predict a surface thickness, it is not a monolayer stabilized simply by the lower surface energy of Cr: the Cr-rich region is many atoms thick.

The nucleation of precipitates at the surface is predicted even in vacuum by this model: of course in real applications of the FeCr alloys the upper layer is oxidized, and so the energy of Cr atoms at the surface depends on the chemical potential: we do not introduce another parameter to fit this external boundary condition.

Although one would expect different interactions at the surface compared to the bulk, the picture emerging from the model is clear: the stainless-steel effect (Cr segregation) will only occur for concentrations in the miscibility gap. Once the Cr-rich surface region is established, it will thicken slowly by diffusion so that the surface can withstand loss of oxide due to wearing.

Many models assume that single atom Cr segregation (as opposed to precipitation) is energetically favored at the surface. Such a segregation effect would imply that the stainless effect should be present for any Cr concentration. The present picture of precipitation requires the alloy to be in the miscibility gap before the stainless effect occurs, which is consistent with the experimental facts.

IV. STABILIZING A HIGH-TEMPERATURE ORDERED PHASE

Having established the correct solubility of Cr in Fe, we now show how high-T precipitates can be stabilized in a way applicable to KMC. Since we wish to describe precipitation on a lattice, while preserving the spatial correlations of the microstructure, the phase must be represented by an ordered structure compatible with the bcc lattice. Here we use the simplest, B2, as a proxy for sigma. This means that the topology of neighbors in the high-temperature phase is not the same as the sigma phase of the FeCr system. While this is

TABLE I. Energies of pure states in the fifth-neighbor model, $A_{58}=5$, $B=6$. The AFM structure is layered in the (001) direction.

System	Composition	Energy	Structure	Magnetism
α	Fe	−58	bcc	Ferro
α'	Cr	−50	bcc	Antiferro
Sigma	FeCr	−48	Sigma	Para
α	$Fe_{15}Cr$	−58	Degenerate	Antiferri

undesirable, the current generation of interatomic potentials allowing off-lattice relaxation does not stabilize *any* high-temperature phase and certainly not the observed sigma phase.

To exist at high temperature, the sigma phase must have higher entropy than α/α'. We must be careful not to approximate away its physical origin. Sigma is an ordered phase (though not an ordered line compound), so this additional entropy cannot be configurational.[51] For this reason, the approximation of using the B2 structure as a proxy for the sigma phase does not remove the key physics.

The electronic structures around an atom are different in sigma from those in α/α'. This could be sensibly described by a local density of states in a *d*-band tight-binding model, from which the energy depends primarily on the local topology and number of electrons. The energy will depend on both spin and species, and since the exchange energy and band structure are different in sigma from α/α', we expect both spin and species contributions to the Hamiltonian to be different. To represent sites which have such a different local electronic structure, an additional variable, p_i, is introduced on each site. This labels whether sites are in the sigma phase ($p_i=1$) or not ($p_i=0$).

Knowing that the sigma phase is paramagnetic, we assume that interactions involving $p_i=1$ sites are spin independent. Then, for ordering interactions within pure sigma phase (all atoms having $p_i=1$), we adopt the simplest model for an alloy, the Ising model itself with a single coupling constant, B. We can then adjust this parameter to set the phase-transition temperature between sigma and α/α'.

The revised Hamiltonian is then

$$H_i(58) = (1-p_i)H_i^0(58) + Bp_i\sum_{j=1}^{8} p_j(S_iS_j), \tag{3}$$

where 58 represents the spin coupling to five neighbor shells and 8 represents the nearest-neighbor interactions that describe the sigma phase [Eq. (3)]. The parameter B represents the relative interaction strengths. In keeping with the spirit of avoiding detailed fitting, we choose the largest integer giving sigma lower energy than either α or α', i.e., $B=6$. The $T=0$ cohesive energies of the stoichiometric structures are given in Table I, wherein sigma is clearly unstable with respect to the pure elements at $T=0$. Other $T=0$ features are that isolated Fe has an energy of −10 in Cr (positive heat of solution) while isolated Cr in Fe has a binding energy of −58 (negative heat of solution). Thus the asymmetry of the miscibility gap is ensured, with $N=58$ making it possible to reach a concentration of 6.25% without introducing neighboring Cr atoms. We note that this general AFM/FM/PM model can be made to produce other ordered ground-state phases with different values of A and B.

To investigate finite temperature we simulate the system using Metropolis Monte Carlo with 54 000 sites (30^3 conventional bcc cells). For the Hamiltonian in Eq. (3) the combined Glauber and Kawasaki dynamics for canonical simulations [Eq. (2)] are combined with an additional trial move $p_i \rightarrow 1-p_i$

Interfacial energies can suppress phase coexistence due to hysteresis and finite-size effects. We finesse this by running two types of calculation: constant concentration canonical and fixed-T grand canonical. We avoid hysteresis by stepping the temperature and restarting the system from cold. With constant concentration we identify the hysteresis regions as those where the ensemble-averaged energy has two branches with changing temperature. For grand-canonical calculations the Hamiltonian becomes

$$H = \sum_i H_i(58) + \mu \sum S_i, \tag{4}$$

wherein the system runs to equilibrium with trial moves as before, then the chemical potential μ is incremented to vary the concentration. At equilibrium, the grand-canonical calculations give a single-phase state, and the concentration at which this phase changes determines the phase boundary.

In practice, it is important to start the grand-canonical calculations with coexisting pure phases: otherwise α' forms AFM domains, which do not anneal out on the time scale of the simulations despite having higher free energy than the single domain.

Checks exist on the realism of using a simple Ising model for the sigma phase: B must be large enough to ensure that the phase remains ordered across its stability range, yet small enough to prevent it being stable down to 0 K. There is no guarantee that these independent constraints can both be met, and so it is encouraging to find that they can be. Similarly, the sigma and bcc-based phases must phase segregate if the notion of a crystal structure at a particular site is to make sense. Again, it is encouraging to find that this does happen. The additional entropy which stabilizes the sigma phase in the model comes from the spin degeneracy associated with the structural label p_i.[52]

As well as representing the sigma phase in precipitates, $p_i=1$ sites may exist at high temperatures in α or α' regions. Following from Eq. (3), they have zero energy; this increases the entropy of the paramagnetic phase, lowering T_C and T_N.

Six quantities are measured as functions of temperature and concentration: mean energy, spin, proportion of p_i, and their rms fluctuations. Phase boundaries are then found from divergences (in practice peaks) in the fluctuations and identified from the σ and p concentration and fluctuation. Snapshots are shown in Fig. 3 and the phase diagram is shown in Fig. 4. It can be seen to contain all the main features of the experimental FeCr diagrams.[1–3]

The pure elements have Curie and Néel temperatures of $T=27.8$(Fe) and $T=19.6$(Cr). These temperatures are lower than the H^0 system because of the entropy associated with

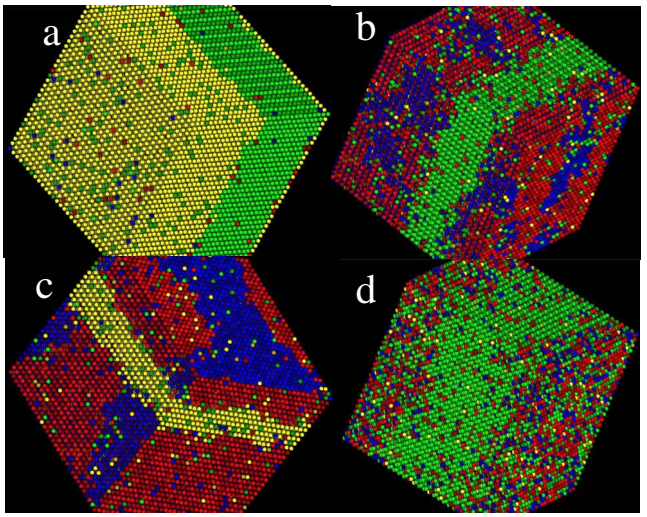

FIG. 3. (Color online) Microstructures formed at various temperatures and concentrations imaged using BALLVIEWER (Ref. 44). For clarity, cases where both phases percolate through the periodic boundaries have been chosen rather than those with spherical precipitates of the minority phase. Color scheme shows bcc Fe ($S_i=1$, $p_i=0$) as yellow and bcc Cr ($S_i=1$, $p_i=0$) as green. Sigma phase atoms are shown as blue (Fe, $S_i=1, p_i=1$) or red (Cr $S_i=0, p_i=1$). Spin state is depicted by light or dark. (a) $\alpha-\alpha'$ coexistence, showing skew solubility $T=9$, $Fe_{0.5}Cr_{0.5}$, (b) α'-sigma coexistence $T=12$, $Fe_{0.3}Cr_{0.7}$, (c) α-sigma phase coexistence $T=12$, $Fe_{0.58}Cr_{0.42}$, and (d) AFM+PM $T=15$, $Fe_{0.15}Cr_{0.85}$. It should be noted that in (c) the apparently distinct red and blue regions are simply different terminations of the B2 structure, separated by an antiphase boundary.

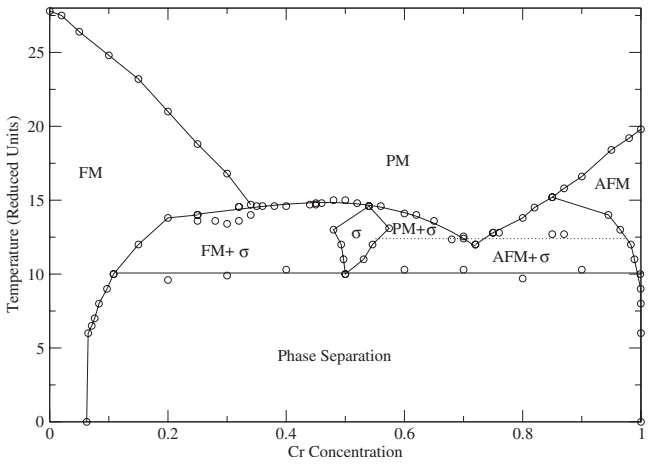

FIG. 4. Phase diagram for sigma phase Hamiltonian in Eq. (3). Points are found from peaks in the heat capacity from Monte Carlo (MC) simulation with 54 000 bcc sites and 10 000 sweeps of the lattice at each temperature. Concentration is held fixed and temperature is incremented in units of 0.1. Additional points are extracted from grand-canonical simulations on the same system, increasing the chemical potential in steps of 0.1 at constant temperature and plotting the concentration at which the system switches across the mixed-phase region. In general, the former method is better for points on "horizontal" lines (e.g., order-disorder) and the latter for "vertical" lines (e.g., edges of phase-coexistence regions). Lines are guides for the eyes separating phase regions. Phase designations FM, AFM+sigma, etc., are deduced from inspection of snapshots (Ref. 44) in the center of the region. The dotted line links the eutectoid to the sigma and AFM phases.

the p label. The modeled sigma phase appears at only high temperatures, above $T=10$, stabilized by the higher entropy arising from the degeneracy between $\sigma=\pm 1$. As temperature increases further, a site-disordered phase appears.

Compared with the actual FeCr and FeV phase diagram there are minor differences: notably the high Néel temperature means that sigma coexists with AFM α' below $T=12$ and a site-disordered phase above $T=12$. This is shown by the dotted line in Fig. 4. Such regions do not appear on most Fe-Cr phase diagrams, although there is some experimental evidence of such a eutectoid[2] for the Fe-rich region.

V. CONCLUSIONS

In summary, we set out to produce a lattice-based model which could reproduce the unusual features of the experimental phase diagram of FeCr. We set ourselves the constraint that it should be lattice based, such that it would be usable in large-scale KMC calculations.

We then obtained a lattice-based Monte Carlo model which gives qualitative explanation for three anomalous properties of FeCr alloys: skew solubility due to short-ranged order, the high-Cr content required for stainless steels, and appearance of high-T ordered phase.

A parametrization inspired by the FeCr system uses pairwise FM-AFM long-range interactions to reproduce the skew solubility without recourse to many-body terms in a cluster expansion. It also predicts surface segregation only in the phase coexistence region.

A nice side effect is the explanation of the stainless-steel effect: surface segregation of Cr is not thermodynamically stable outside the miscibility gap. In the miscibility gap Cr precipitates grow preferentially on the surface. This provides a qualitative explanation for the fact that the stainless-steel effect is only observed for relatively large Cr concentrations (typically greater than 12% Cr).

The same ($N=58$) model produces high-T sigma precipitation. Preliminary tests show that the same effects are obtained with a short-range H^0 model. This shows that the sigma phase is not stabilized by the same long-range interactions which give anomalous stability but rather by the excess paramagnetic contribution to the entropy. The model Hamiltonian is very simple to compute, easily generalized to other systems, and will enable KMC simulations of precipitation on a time scale of years.

ACKNOWLEDGMENTS

The author acknowledges support from the EPSRC under Grants No. GR/S81186/01 and No. GR/T11753/01 and the EU GETMAT project.

*gjackland@ed.ac.uk

[1] H. Okamoto, in *Binary Alloy Phase Diagrams II*, 2nd ed., edited T. B. Massalski (ASM International, Metals Park, OH, 1990), Vol. 2, p. 1271.

[2] E. Z. Vintaykin, V. Y. Kolontsov, and E. A. Medvedev, Russ. Metall. **4**, 109 (1969).

[3] J. R. Davis, *ASM Spectroscopy Handbook: Stainless Steels* (ASM, Materials Park, OH, 1994).

[4] M. K. Miller, J. M. Hyde, M. G. Hetherington, A. Cerezo, G. D. W. Smith, and C. M. Elliott, Acta Metall. Mater. **43**, 3385 (1995).

[5] M. Hennion, J. Phys. F: Met. Phys. **13**, 2351 (1983).

[6] P. Olsson, I. A. Abrikosov, L. Vitos, and J. Wallenius, J. Nucl. Mater. **321**, 84 (2003).

[7] T. P. C. Klaver, R. Drautz, and M. W. Finnis, Phys. Rev. B **74**, 094435 (2006).

[8] D. Nguyen-Manh, M. Yu. Lavrentiev, and S. L. Dudarev, J. Comput.-Aided Mater. Des. **14**, 159 (2007).

[9] A. V. Ruban, P. A. Korzhavyi, and B. Johansson, Phys. Rev. B **77**, 094436 (2008).

[10] J. M. Hyde, A. P. Sutton, J. R. G. Harris, A. Cerezo, and A. Gardiner, Modell. Simul. Mater. Sci. Eng. **4**, 33 (1996).

[11] G. J. Ackland and V. Vitek, Philos. Mag. B **62**, 149 (1990).

[12] B. Fultz, L. Anthony, J. L. Robertson, R. M. Nicklow, S. Spooner, and M. Mostoller, Phys. Rev. B **52**, 3280 (1995).

[13] A. Caro, D. A. Crowson, and M. Caro, Phys. Rev. Lett. **95**, 075702 (2005).

[14] P. Olsson, J. Wallenius, C. Domain, K. Nordlund, and L. Malerba, Phys. Rev. B **72**, 214119 (2005).

[15] J. Wallenius, I. A. Abrikosov, R. Chakarova, C. Lagerstedt, L. Malerba, P. Olsson, V. Pontikis, N. Sandberg, and D. Terentyev, J. Nucl. Mater. **329-333**, 1175 (2004).

[16] M. I. Mendelev, S. Han, W. J. Son, G. J. Ackland, and D. J. Srolovitz, Phys. Rev. B **76**, 214105 (2007).

[17] P. Olsson, J. Wallenius, C. Domain, K. Nordlund, and L. Malerba, Phys. Rev. B **72**, 214119 (2005).

[18] G. J. Ackland and S. K. Reed, Phys. Rev. B **67**, 174108 (2003).

[19] G. J. Ackland, J. Nucl. Mater. **351**, 20 (2006).

[20] A. E. Kissavos, S. M. Simak, P. Olsson, L. Vitos, and I. A. Abrikosov, Comput. Mater Sci **35**, 1 (2006).

[21] E. M. Lopasso, M. Caro, A. Caro, and P. E. Turchi, Phys. Rev. B **68**, 214205 (2003).

[22] J. J. Blackstock and G. J. Ackland, Philos. Mag. A **81**, 2127 (2001).

[23] P. Erhart, A. Caro, M. Serranode Caro, and B. Sadigh, Phys. Rev. B **77**, 134206 (2008).

[24] G. Bonny, P. Erhart, A. Caro, R. C. Pasianot, L. Malerba, and M. Caro, Modell. Simul. Mater. Sci. Eng. **17**, 025006 (2009).

[25] P. E. A. Turchi, G. M. Stocks, W. H. Butler, D. M. Nicholson, and A. Gonis, Phys. Rev. B **37**, 5982 (1988).

[26] M. Yu. Lavrentiev, R. Drautz, D. Nguyen-Manh, T. P. C. Klaver, and S. L. Dudarev, Phys. Rev. B **75**, 014208 (2007).

[27] G. J. Ackland, Phys. Rev. Lett. **97**, 015502 (2006).

[28] P. E. A. Turchi, L. Reinhard, and G. M. Stocks, Phys. Rev. B **50**, 15542 (1994).

[29] M. Sluiter and P. E. A. Turchi, Phys. Rev. B **46**, 2565 (1992).

[30] P. Erhart, B. Sadigh, and A. Caro, Appl. Phys. Lett. **92**, 141904 (2008).

[31] R. L. Klueh, Curr. Opin. Solid State Mater. Sci. **8**, 239 (2004).

[32] A. Kimura, Mater. Trans. **46**, 394 (2005).

[33] K. Tsuzuki *et al.*, Nucl. Fusion **43**, 1288 (2003).

[34] W. M. Young and E. W. Elcock, Proc. Phys. Soc. London **89**, 735 (1966).

[35] F. Soisson, J. Nucl. Mater. **349**, 235 (2006).

[36] Sigma is spelled out in full to avoid confusion with the symbol for spin.

[37] G. Bergman and D. P. Shoemaker, Acta Crystallogr. **7**, 857 (1954).

[38] G. Bergman and D. P. Shoemaker, Acta Crystallogr., Sect. B: Struct. Sci. **52**, 777 (1996).

[39] D. A. Read, E. H. Thomas, and J. B. Forsythe, J. Phys. Chem. Solids **29**, 1569 (1968).

[40] J. Cieslak, B. F. O. Costa, S. M. Dubiel, M. Reissner, and W. Steiner, J. Phys. Condens. Matter **17**, 6889 (2005).

[41] J. Cieslak, B. F. O. Costa, S. M. Dubiel, M. Reissner, and W. Steiner, J. Phys. Condens. Matter **17**, 2985 (2005).

[42] M. H. F. Sluiter, K. Esfarjani, and Y. Kawazoe, Phys. Rev. Lett. **75**, 3142 (1995).

[43] This is true if one assumes that the energy is a sum of pairwise interactions. If the interaction is an embedded-atom-type nonlinear function of a sum of pair potentials, the interaction needs to extend only to second neighbors.

[44] G. J. Ackland and A. P. Jones, Phys. Rev. B **73**, 054104 (2006).

[45] B. Nonas, K. Wildberger, R. Zeller, and P. H. Dederichs, Phys. Rev. Lett. **80**, 4574 (1998).

[46] W. T. Geng, Phys. Rev. B **68**, 233402 (2003).

[47] A. V. Ruban, H. L. Skriver, and J. K. Norskov, Phys. Rev. B **59**, 15990 (1999).

[48] A. V. Ponomareva, E. I. Isaev, N. V. Skorodumova, Yu. Kh. Vekilov, and I. A. Abrikosov, Phys. Rev. B **75**, 245406 (2007).

[49] A. Kiejna and E. Wachowicz, Phys. Rev. B **78**, 113403 (2008).

[50] P. A. Dowben, M. Grunze, and D. Wright, Surf. Sci. **134**, L524 (1983).

[51] Note that the sigma phase is not an ordered compound in the strict sense of having only one composition—both in the model and in real FeCr, there is a range of composition within which the sigma phase exists. In addition, the sigma phase is a complex phase with five sublattices, and configurational disorder exists on some sublattices: this does give rise to some configurational entropy but not of itself enough to stabilize the phase.

[52] The interpretation of the additional entropy coming from paramagnetism should not be taken too literally. In such a simple model the σ degeneracy captures all spin, phonon, and electronic contributions to the excess entropy, while the p label incorporates all bonding contributions, including the implicit lattice rearrangement from B2 to sigma.